

# Roll-to-roll tomographic volumetric additive manufacturing for continuous production of microstructures on long flexible substrates

Joseph Toombs<sup>a</sup>, Chi Chung Li<sup>a</sup>, Hayden Taylor<sup>a</sup>

<sup>a</sup>Dept. of Mechanical Engineering, University of California, Berkeley, CA USA 94704

## ABSTRACT

Tomographic volumetric additive manufacturing (VAM) has proven viable to 3D-print diverse materials including polymer, glass, ceramic, and hydrogel at the centimeter scale. As tomographic VAM is extended to the microscale, many of its advantages are translatable, including smooth layer-less surfaces, support-free and shear force-free printing, material flexibility, and speed of production. However, as we shrink the patterning scale, the depth of field shrinks much more rapidly and does so roughly with the square of the patterning scale. Consequently, the build volume is substantially reduced as the numerical aperture of the system is increased. Additionally, microscale tomographic VAM is currently limited to batch production, i.e., the photoresist container must be exchanged after the exposure phase is completed. In this work, we introduce roll-to-roll (R2R) tomographic VAM in which these limitations are addressed by “unwrapping” the precursor material into a film enabling continuous production of microstructures with theoretically unlimited length. We elaborate the design of a focus-multiplexed projection optical system that can scan the projection focal plane axially in sync with the refresh cycle of a digital micromirror device. We describe the process of iteratively optimizing and segmenting sinograms to produce long aperiodic microstructures with the focus tunable optical system. Furthermore, we formulate a thermally reversible organogel photoresist which is deposited onto the substrate in films multiple millimeters in thickness with slot-die coating. Finally, we present progress on printing with the R2R tomographic VAM system.

**Keywords:** tomographic volumetric additive manufacturing, roll-to-roll processing, photopolymerization, 3d printing, microfabrication

## 1 INTRODUCTION

Compared to stereolithography and digital light processing 3D printing, volumetric additive manufacturing (VAM) is advantageous because photoresist recoating steps and suction forces are eliminated, the ability to embed premanufactured functional objects in the precursor material is gained, and geometric flexibility is high as sacrificial supports are not required for many structures. Several VAM methods have demonstrated high printing resolution with sub-micron minimum feature size possible. However, it is challenging to scale these methods in such a way that this local resolution is maintained on objects with large overall dimensions due to specialized optical systems and/or requirements for high photoresist optical transmission at the actinic wavelength.<sup>1</sup>

Computed axial lithography (CAL) is a VAM method which enables 3D printing of whole objects volume-at-once with high geometric flexibility<sup>2,3</sup>. In our previous work, we have printed objects with minimum feature size of 20  $\mu\text{m}$  in a free-radical polymerization photoresist with a refined system called micro-CAL<sup>4</sup>. Improvement in printing resolution in CAL, however, comes at the cost of substantially reduced build diameter; the maximum usable diameter is restricted by the tolerable defocus of the projection optical system (even if the lateral size of the image is larger than this value). Objects with large cross-section and small feature size are difficult to produce with micro-CAL. Furthermore, it is typical to expose the photoresist over several rotations, so printing is generally limited to batch production.

A linear translational volumetric 3D printing process called xolography is made possible by the use of photochromic sensitization of a photoinitiator<sup>5</sup>. A light sheet of one color sensitizes a plane of photoresist and an orthogonally propagating cross-sectional image of an object of another color initiates polymerization. In the seminal work, the photoresist was translated relative to the stationary light sheet. However, in a second implementation, the photoresist was instead pumped through a specially designed flow cell to extend the build volume along the direction of flow to infinity, theoretically<sup>6</sup>. In this configuration, objects with minimum lateral feature size of 10  $\mu\text{m}$  were printed at speeds up to 3.5  $\text{mm min}^{-1}$ . Although xolography is a flexible process, it requires special types of photoinitiators, a dual-wavelength projection system, and dual-wavelength transmission of the photoresist.

At a smaller scale, for two-photon polymerization (2PP), typically either the photoresist or objective lens is translated by a piezo stage. Piezo elements have limited range and, thus, to extend printing height a larger coarse stage must be combined with or take the place of the piezo stage. However, 2PP has been adapted to continuous fabrication with clever microfluidic delivery of fresh photoresist. Long microtubule scaffolds (100:1 aspect ratio) for vascular tissue engineering were printed at speeds of  $12.5 \mu\text{m s}^{-1}$  in a vertical flow microfluidic chip<sup>7</sup>. Furthermore, 3D colloidal microparticles were printed in a horizontal flow channel at rates of 30 particles per second<sup>8</sup>. These continuous printing architectures require femtosecond lasers to achieve volumetric patterning which are expensive and require amplification if optically expanded to large-scale cross sections for advanced, high-throughput techniques.

Roll-to-roll (R2R) production, the peak of low-cost, high-throughput continuous manufacturing, of relatively thin, featureless flat structures includes various standard manufacturing operations like coating, lamination, and drying steps. However, applications including refractive optics or diffractive light guides, fluid management, dry adhesive, and filtration require formation of 3D features in the functional layer. These are formed by molding/embossing and gravure processes which do not permit complex geometry like reentrant and overhanging features. A process module that could be integrated into a line and that enables fabrication of these structures would result in enhanced capabilities and faster adoption of scalable R2R manufacturing.

We present a novel polymer patterning scheme called R2R CAL which combines R2R processing with the light-based tomographic printing approach of conventional CAL to create 3D structures without supports within a layer of photoresist on a flexible substrate. R2R CAL exploits free-radical polymerization inhibition and, therefore, does not require an expensive femtosecond laser source or specialized dual color photoinitiator to achieve continuous volumetric photopolymerization.

## 2 METHODOLOGY

### 2.1 Concept of R2R CAL

A CAL system with high numerical aperture and short depth of focus has a small build volume where the tomographic point spread function (PSF) is near-uniform. Several concepts have been introduced to access larger build volume. A non-telecentric projection architecture expands the addressable volume by increasing the lateral size of the projected image. The projected image can be substantially larger than the diameter of the largest optical element, but, in this configuration, “layers” of the build volume can no longer be assumed independent of each other. Propagation models used to simulate dose accumulation and optimize projection images should be generalized to accommodate, for example, a light ray emanating from a projected pixel that passes through several layers<sup>9</sup>. Relative motion of the photoresist and the optical system along the vector defining the rotation axis extends the addressable volume along said direction. This is a form of time multiplexing of the projected images such that the source follows a helical path<sup>10</sup>. Both above approaches may be combined to further expand the build volume.

The R2R CAL concept is a departure from the previous concepts because instead of extending the build volume along the height axis, we observe that the perimeter of the photoresist volume can be “unwrapped” into a continuous strip. When supplied fresh photoresist on a web, the process can be adapted to a continuous process. However, a ramification of adopting this configuration is that the projection illumination cannot completely encircle the photoresist and the requisite light dose must be reached in less than one rotation of the material.

Orlov’s condition proves completeness for inversion of projection in computed tomography when the source-detector unit vector sweeps a line connecting two opposite points on the unit sphere<sup>11</sup>. In a Fourier interpretation, from the central slice theorem, complete coverage of  $k$ -space is required to guarantee inversion without artifacts. Given sufficiently high angular sampling, if the Orlov’s condition is satisfied, any geometry can be reconstructed without streak artifacts. In principle, the same condition applies to CAL, except that non-negativity of projection patterns implies imperfect tomogram contrast and homogeneous material attenuation (due to active or passive absorption e.g. photoinitiator or scattering) further constrains the reproducible spatial frequency coverage.

In the R2R CAL configuration, the wrapped portion of photoresist is exposed to images directed along a projection vector which sweeps a great semicircle source trajectory on Orlov’s sphere. In an ideal scenario where there is no refraction at the photoresist-medium interface, this trajectory is a complete semicircle. However, if the medium has smaller index of refraction than the photoresist (e.g. air-photoresist interface), refraction at the interface is equivalent to a reduction in the

arc length of the source trajectory or a reduction in k-space coverage. In previous work, we have demonstrated empirically that this reduction is not detrimental to optimum tomogram fidelity as long as the k-space representation of the target geometry is sufficiently covered<sup>12</sup>.

Conceptually, there are two relevant domains in R2R CAL (Figure 1). First, the “wrapped” domain describes the state of the photoresist and substrate when it is bearing on a cylindrical face. Second, the “unwrapped” domain refers to the photoresist and substrate when it is in a flat state, i.e., not wrapped on a cylindrical support. The target can be defined in either domain but given that many relevant structures are flat, e.g., filters, flexible electronics, microfluidic devices, and metasurfaces/metamaterials, we have chosen the more natural framework, to define the target in the unwrapped domain.

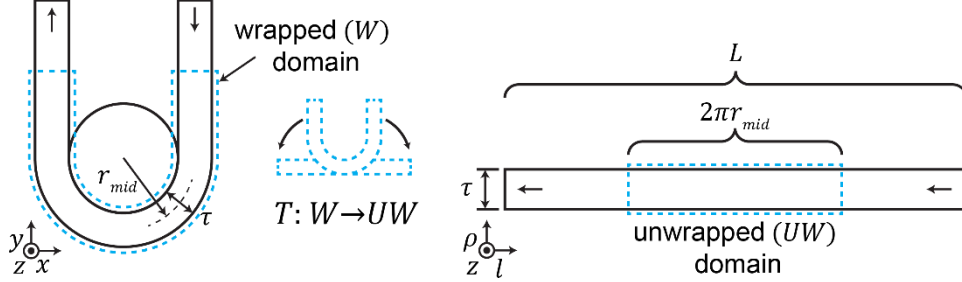


Figure 1. Transformation in tomogram domain from the wrapped to unwrapped domain. The unwrapped domain only covers a subset of the longer possible tomogram domain.

## 2.2 Mathematics and algebraic representation

In conventional CAL, the target and projection domains (or tomogram and sinogram space, respectively, as referred to in computed tomography literature) are the paired spaces where the virtual model to be printed and the digital images projected to photopolymerize the model reside, respectively. The target model is specified in the dimensions that it should be printed. Simulated backprojections are accumulated in the target domain and compared directly to the prescribed target model and dose. In R2R CAL, however, there is a minor yet important difference. The tomogram domain is instead represented by two different domains i.e. wrapped and unwrapped, each with a different purpose to facilitate optimization or target definition.

First, in the context of the physical setup, accumulation of light dose occurs when the web passes over a roller and the photoresist is in a “wrapped” shape with semicircular profile. Accordingly, simulated propagation of projected light including refraction, attenuation, and absorption occurs in this domain. In conventional CAL, forward propagation is performed algebraically as  $\underline{P}\underline{f} = \underline{g}$  where  $\underline{P}$  is the propagation matrix,  $\underline{f}$  is the optical dose, and  $\underline{g}$  is the sinogram. Dose coefficients of  $\underline{P}$  are calculated with Eikonal ray tracing<sup>13</sup>. Note that  $\underline{P}$  represents projection from all angles simultaneously.

For an infinitely long patterning system in R2R CAL, the propagation matrix is also infinitely large. Here, we leverage the shift invariance in the system to represent the overall propagation matrix using only coefficients from one angular projection where  $\underline{P}_{f \rightarrow g}$  is the shift-invariant projection matrix from the wrapped domain to sinogram space. In conjunction with a translation (shifting) operator, we can then repeatedly use these coefficients to compute the overall operation of  $\underline{P}$ . Further, instead of infinite length, we limit the length of the shifting window to be equal to the circumference of the exposure roller (described in section 2.3) in the current implementation. In a sense, this is analogous to a change in the target prescription dose as a function of angle with a single shift-invariant projection operator. Note the difference from conventional CAL, where the target is unchanging with angle in the tomogram domain (Table 1).

Second, the “unwrapped” domain is needed because it represents the actual state of the printed object after light exposure is completed in the wrapped domain. Since the target is defined in the unwrapped domain, the light dose should also be accumulated and compared to the prescription dose here. Therefore, a remapping is needed to transform between the unwrapped and wrapped domains in order to complete the forward and backprojection models. Figure 2 ( $P$  projection operator) shows the dose coefficients in each domain when attenuation is  $\alpha = 0.6\tau^{-1}$  and the refractive index of the photoresist and immersion medium are equal. The overlaid “rays” are helpful to visualize how a sample pattern is backprojected in each domain.

Table 1. Algebraic propagation in conventional CAL vs R2R CAL

	Propagation matrix	Optical dose	Sinogram
Conventional CAL	$N_\theta \cdot N_r \begin{bmatrix} N_x \cdot N_y \\ \underline{\underline{\mathbf{P}}}_{f \rightarrow g} \end{bmatrix}$	$N_x \cdot N_y \begin{bmatrix} 1 \\ \underline{\underline{\mathbf{f}}} \end{bmatrix}$	$N_r \cdot N_\theta \begin{bmatrix} 1 \\ \underline{\underline{\mathbf{g}}} \end{bmatrix}$
R2R CAL	$N_r \begin{bmatrix} N_x \cdot N_y \\ \underline{\underline{\mathbf{P}}}_{f_{UW} \rightarrow g} \end{bmatrix}$	$N_x \cdot N_y \begin{bmatrix} N_\theta \\ \underline{\underline{\mathbf{f}}}_{\theta_0} \dots \underline{\underline{\mathbf{f}}}_{\theta_N} \end{bmatrix}$	$N_r \begin{bmatrix} N_\theta \\ \underline{\underline{\mathbf{g}}}_{\theta_0} \dots \underline{\underline{\mathbf{g}}}_{\theta_N} \end{bmatrix}$

To simplify and reduce the number of operations, the transformation is subsumed into the propagation matrix. Specifically, dose coefficients in the wrapped domain are mapped to the unwrapped domain in the transformation  $T: W \rightarrow UW$  (shown pictorially in Figure 1) as follows

$$\begin{aligned}
 P_{f_W \rightarrow g} f_W &= g \\
 T_{W \rightarrow UW}(P_{f_W \rightarrow g}) f_{UW} &= g \\
 P_{f_{UW} \rightarrow g} f_{UW} &= g.
 \end{aligned}$$

The result is a propagation operator,  $P_{f_{UW} \rightarrow g}$ , which enables projection from the target (or intermediate dose during iterative optimization) in the unwrapped domain to the sinogram with a single matrix-vector multiplication. The adjoint of  $P_{f_{UW} \rightarrow g}$ ,  $P_{f_{UW} \rightarrow g}^*$ , gives the backpropagation from the sinogram to the optical dose in the unwrapped domain. Furthermore, the forward propagation matrix,  $\underline{\underline{\mathbf{P}}}_{f_{UW} \rightarrow g}$ , and backpropagation matrix,  $\underline{\underline{\mathbf{P}}}_{f_{UW} \rightarrow g}^*$ , can be reused along the z-axis since each slice is independent under the assumption of small etendue and that propagating rays remain within a plane.

Since  $\underline{\underline{\mathbf{P}}}_{f_{UW} \rightarrow g}$  represents propagation from a fixed angle, web motion and corresponding change in target relative to the projection vector is expressed as change in tomogram domain, where  $\underline{\underline{\mathbf{f}}}_{\theta_i}$  is a view of the tomogram at an instant in time or angle. Because the unwrapped domain only covers a subset of a possibly longer tomogram space, blocks of the tomogram are extracted with the sliding-window unfold function in PyTorch as  $\underline{\underline{\mathbf{f}}}_{\theta_0} \dots \underline{\underline{\mathbf{f}}}_{\theta_N}$ . The matrix-matrix product of  $\underline{\underline{\mathbf{P}}}_{f_{UW} \rightarrow g}$  and the matrix formed by  $\underline{\underline{\mathbf{f}}}_{\theta_0} \dots \underline{\underline{\mathbf{f}}}_{\theta_N}$  performs forward projection and gives the sinogram. Figure 2 shows this algebraic propagation graphically. The sinogram can be flattened into a vector to maintain compatibility with existing optimization algorithms like band-constraint Lp norm minimization<sup>13</sup>. The reverse process, backprojection, gives the same sequence of blocks that are accumulated in the tomogram domain with the fold function in PyTorch.

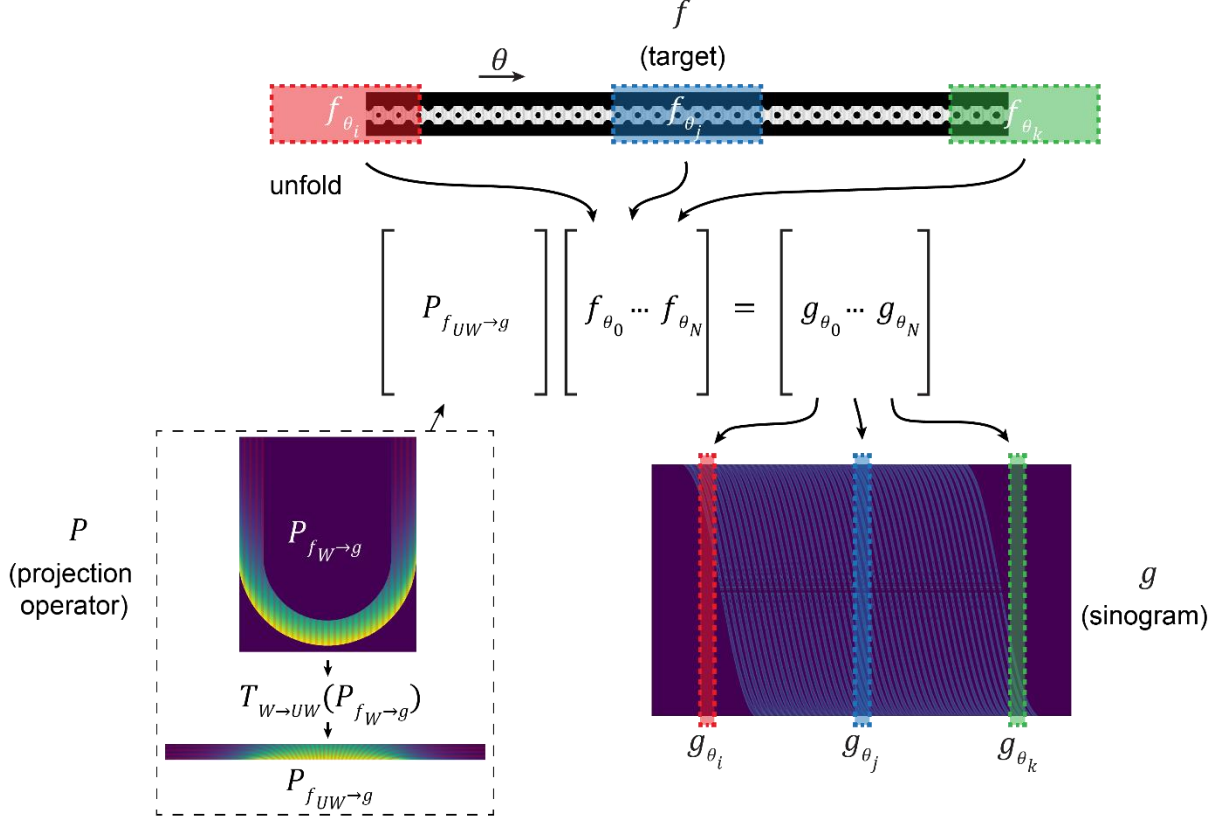


Figure 2. Algebraic propagation in R2R CAL.  $f_{\theta_i}$  is a view of the target or tomogram  $f$  at an instant in time or angle depicted as a sliding colored window.  $g_{\theta_i}$  is the corresponding sinogram slice depicted as a colored window of the same color on the sinogram  $g$ .  $P$  is the projection operator which is transformed from the wrapped to the unwrapped domain such that projection directly from  $f_{\theta_i}$  in the unwrapped domain to  $g_{\theta_i}$  is possible. The red overlaid lines depict simulated “rays” from a backprojection.

### 2.3 Apparatus and materials

The purpose of the material handling system is to deposit a uniform coating of photoresist on a web and control motion of the photoresist-coated web through the exposure light. The web feed roller is driven by a closed loop stepper motor and the take-up roller is driven by an AC torque motor. The AC torque motor provides constant torque at stall and low speeds and thus near constant tension in the web. A variable AC power supply powers the torque motor and enables adjustable web tension. The web is 75  $\mu\text{m}$  thick and 63.5 mm wide polyethylene film.

The photoresist is loaded into a heated syringe pump and deposited on the web by pumping through a custom heated slot-die coater. The slot-die coater slot width and gap height are adjustable such that films up to 3 mm in thickness can be coated. In this work, we use a thermally gelling photoresist<sup>14</sup> which is comprised of 92 wt% trimethylolpropane triacrylate monomer and 7 wt% ethyl cellulose thermoplastic binder, 0.5 wt% camphorquinone (CQ) photoinitiator and 0.5 wt% ethyl-4-dimethylaminobenzoate co-initiator. The equivalent concentration of CQ is 0.036 M.

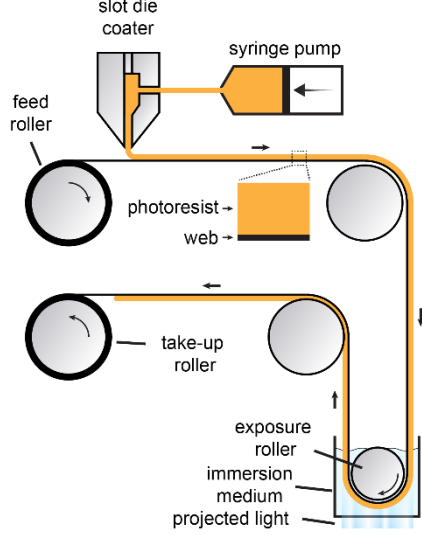


Figure 3. Material handling. The web moves from the feed roller to the take-up roller passing over several idler rollers and the exposure roller where projected light is directed. Photoresist is dispensed onto the moving web through a heated slot-die coater and syringe pump.

The optical system (Figure 4A) is similar to that of our previous work<sup>4</sup>. A 442 nm laser diode is launched into a multimode optical fiber (OF) to homogenize the intensity profile. The output of the fiber is expanded to fill the active portion of the digital micromirror device (DMD). Images from the precomputed sinogram are displayed on the DMD and projected onto the moving photoresist-coated web through a pair of 4f relays. In the Fourier plane of the first 4f relay ( $M_1 = 1$ ), an electrically tunable lens (ETL) is placed. After the second 4f relay ( $M_2 = 1.33$ ), the focal plane position,  $y_0$ , as a function of the optical power of the ETL in diopters,  $D_{ETL}$ , is found by ray transfer matrix analysis to be

$$y_0(D_{ETL}) = n_u \left[ -f_2^2 M_2^2 \left( \frac{D_{ETL}}{1000} + \frac{1}{f_{OL}} \right) + f_4 - y_{air} \right]$$

where  $n_u$  is the refractive index of the immersion medium,  $f_2$  and  $f_4$  are the focal length of L2 and L4 in mm,  $f_{OL}$  is the focal length of the ETL offset lens in mm, and  $y_{air}$  is the distance from L4 to the immersion medium. The ETL has a minimum optical power step size of 0.01 diopters which equates to minimum  $\Delta y = 0.47$  mm. Furthermore, the optical power modulation range is sufficient to scan the focal plane at least the radius of the exposure roller which allows segmented sinogram images to be projected into the wrapped photoresist in focus. Figure 4D shows the change in focal plane position as a function the ETL optical power. A small portion of the total modulation range leads to linear focus tuning  $\geq 10$  mm.

The depth of focus of a projected pixel was measured with a CCD sensor mounted to a motorized linear stage. For a series of images along the propagation axis (Figure 4B), a Gaussian distribution was fit to the pixel grayscale intensity such that the minimum beam waist,  $w_0$ , at the focal plane and the depth of focus,  $b$ , could be determined.  $b$ , measured as the distance where  $w < \sqrt{2}w_0$ , was 3.0 mm and  $w_0 = 13.75$   $\mu\text{m}$ .

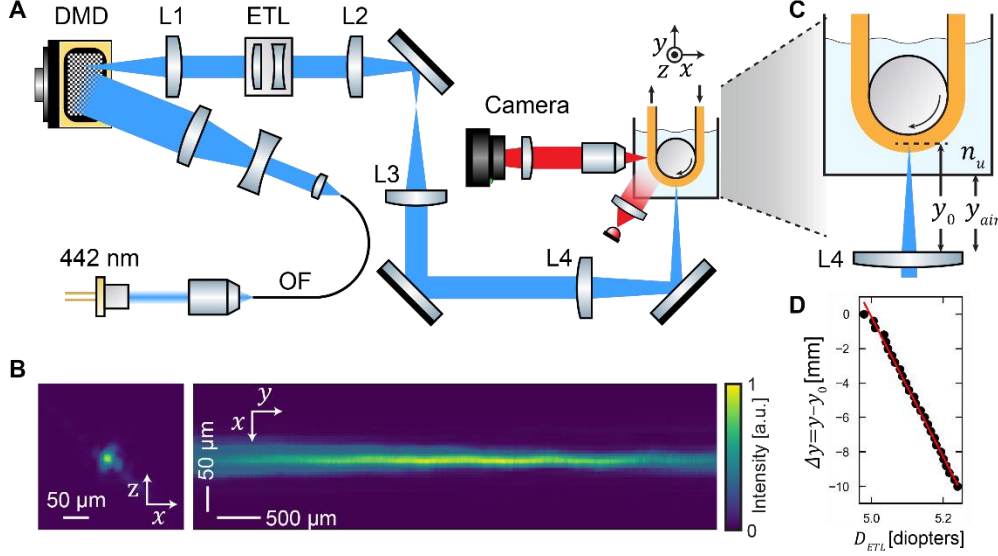


Figure 4. A) Optical system. Precomputed digital light patterns are displayed on the DMD and projected onto the moving photoresist. B) PSF (in air) of the optical system including the ETL. C) Relevant dimensions for tunable focusing. D) Distance of focus from reference,  $\Delta y$ , vs optical power. Red line represents a linear fit to measured focus distance.

### 3 RESULTS AND DISCUSSION

We selected a triply periodic minimal surface (TPMS) to demonstrate printing capabilities. TPMS structures have been used for many applications ranging from filtration<sup>15</sup> to mechanical metamaterials<sup>16</sup>. We used a direct slicing method from the functional representation of the gyroid TPMS to create a voxel representation<sup>17,18</sup>. Two level sets were chosen to define the boundaries between solid and void regions of a shell-type structure. Furthermore, as R2R CAL enables printing of aperiodic geometry, a spatial gradation was applied to change the density of the structure by 50% over a length of 10 cm. The designed geometry with orthographic side and end projections is shown in Figure 5A. The band constraint  $L_p$  norm minimization algorithm was used to optimize digital projection images<sup>13</sup>. The forward projection normalized by the total dose in the backprojection was used as the initial guess. Figure 5B shows a slice of the reconstructed dose response after optimization. The optimized projection images are then loaded onto the DMD and refreshed in sync with the motion of the web. Figure 5C shows projected images propagating through the immersion medium and into the photoresist as the printed structure forms. At the actinic wavelength (442 nm), the photoresist has refractive index<sup>14</sup> of 1.489 and the immersion medium, water, has refractive index of 1.337. Therefore, the maximum angular coverage is  $127^\circ$ . The choice to use water as immersion medium was a practical one; it was substantially easier to keep the web handling system clean due to the high surface tension of water (and minimal wetting of the web) as compared to oil-based immersion media.

The printed structure was removed from the web and developed in a vat of propylene glycol methyl ether acetate heated to approximately  $50^\circ\text{C}$  for 10 minutes. The resulting structure was scanned on a flatbed scanner and it is shown in Figure 5D. The minimum shell thickness is approximately  $250\ \mu\text{m}$  and the total length is 10.1 cm. The printing area is determined by the thickness of the photoresist coating and the maximum width of the projected image. Coating thickness of 3 mm was used, and the maximum projected width is 15.5 mm. The effective printing area was  $46.5\ \text{mm}^2$ . Linear printing rates, i.e., web speed, up to  $48\ \text{mm}\ \text{min}^{-1}$  were achieved which equates to a volumetric printing rate of  $2232\ \text{mm}^3\ \text{min}^{-1}$ .

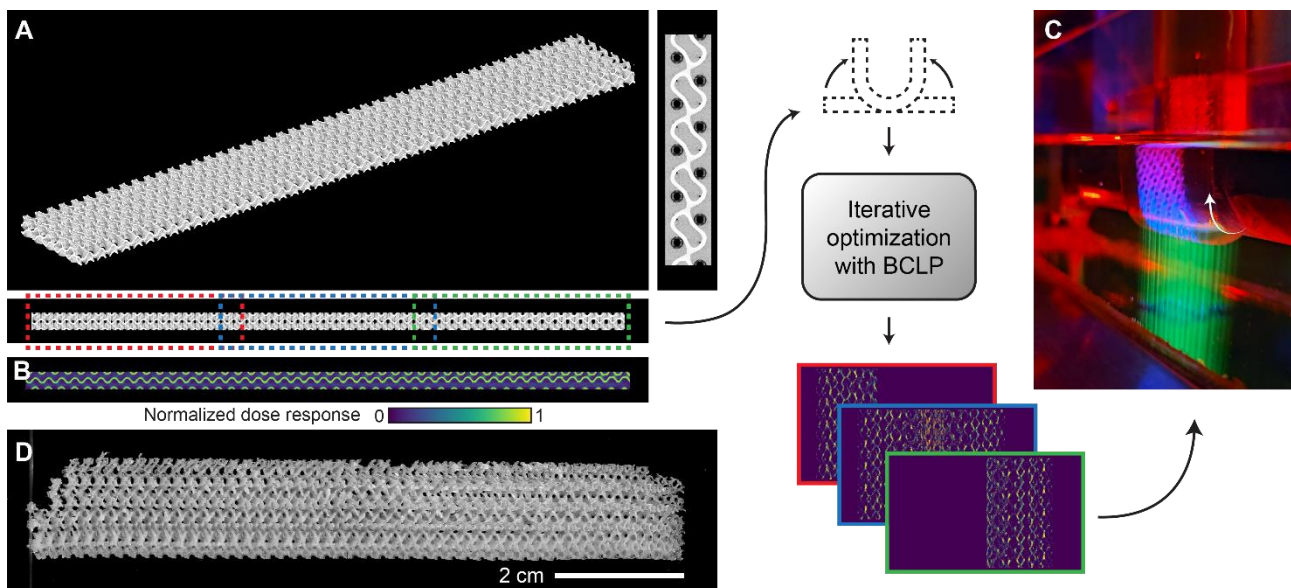


Figure 5. A) Voxel rendering of an aperiodic gyroid triply periodic minimal surface. The sliding window (PyTorch fold function) extracts the portion of the target that represents the unwrapped domain. In iterative optimization, the unwrapped domain is transformed to wrapped domain to perform forward projection. To evaluate the loss function, backprojection in the wrapped domain is transformed back to unwrapped domain. B) Reconstructed normalized dose response. C) Sinogram images are projected in sync with the motion of the web. Fluorescein was added to the immersion medium to cause fluorescence for visualization only. D) Printed structure removed from the web.

In R2R manufacturing, curling phenomena are commonly observed due to the nature of the web’s path over conveyance rollers<sup>19</sup>. In R2R CAL, the photoresist is exposed in the wrapped, or curled, state. After removing from the web and developing several experimental prints, we observed curling distortion along the same axis as the exposure roller. This indicates that during polymerization the curvature of the photoresist was “recorded”, i.e., when flattened, a stress profile develops through the thickness of the printed structure. When removed from the substrate, strain recovery causes the structure to curl. To mitigate this effect, the exposure conditions were adjusted to delay the onset of polymerization until just after the photoresist passed the tangent point between the exposure roller and flattened web (Figure 6).

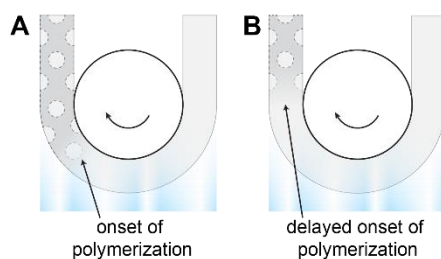


Figure 6. A) If the onset of polymerization occurs when web has curvature, the resulting printed structure will exhibit curling distortion due to strain recovery after it is removed from the web. B) By adjusting exposure conditions, it is possible to delay the onset of polymerization until the web has zero curvature.

Notably, the R2R CAL 3D printing concept is not limited to connected structures. It is possible to optimize for and print arrays of isolated objects. In future work, we will explore the capabilities of the system by printing challenging structures including customized particles and microfluidic devices. We will also explore the potential of this architecture to print polymeric components onto a web with integrated electronics for applications in flexible sensors. Finally, we will take advantage of the curling effect to create objects with shape-morphing capabilities.

## 4 CONCLUSION

R2R CAL is a continuous volumetric 3D printing method which is based on tomographic superposition principles and exploits inhibition behavior in photoresists. We described the computational framework which enables generation of optimized sinograms for long aperiodic structures. We constructed a custom R2R conveyor line and laser-based optical system with focus tunability. Finally, we demonstrated printing of a spatially graded gyroid TPMS structure with overall length of 10.1 cm and minimum feature size of 250  $\mu\text{m}$  and proposed directions of future research to address a wide range of applications.

## REFERENCES

- [1] Thijssen, Q., Toombs, J., Li, C. C., Taylor, H. and Van Vlierberghe, S., “From pixels to voxels: A mechanistic perspective on volumetric 3D-printing,” *Progress in Polymer Science* **147**, 101755 (2023).
- [2] Kelly, B. E., Bhattacharya, I., Heidari, H., Shusteff, M., Spadaccini, C. M. and Taylor, H. K., “Volumetric additive manufacturing via tomographic reconstruction,” *Science* **363**(6431), 1075–1079 (2019).
- [3] Loterie, D., Delrot, P. and Moser, C., “High-resolution tomographic volumetric additive manufacturing,” *Nature Communications* **11**(1), 852 (2020).
- [4] Toombs, J. T., Luitz, M., Cook, C. C., Jenne, S., Li, C. C., Rapp, B. E., Kotz-Helmer, F. and Taylor, H. K., “Volumetric additive manufacturing of silica glass with microscale computed axial lithography,” *Science* **376**(6590), 308–312 (2022).
- [5] Regehly, M., Garmshausen, Y., Reuter, M., König, N. F., Israel, E., Kelly, D. P., Chou, C.-Y., Koch, K., Asfari, B. and Hecht, S., “Xolography for linear volumetric 3D printing,” *Nature* **588**(7839), 620–624 (2020).
- [6] Stüwe, L., Geiger, M., Röllgen, F., Heinze, T., Reuter, M., Wessling, M., Hecht, S. and Linkhorst, J., “Continuous Volumetric 3D Printing: Xolography in Flow,” *Advanced Materials*, 2306716 (2023).
- [7] Lölsberg, J., Cinar, A., Felder, D., Linz, G., Djeljadini, S. and Wessling, M., “Two-Photon Vertical-Flow Lithography for Microtube Synthesis,” *Small* **15**(33), 1901356 (2019).
- [8] Shaw, L. A., Chizari, S., Shusteff, M., Naghsh-Nilchi, H., Di Carlo, D. and Hopkins, J. B., “Scanning two-photon continuous flow lithography for synthesis of high-resolution 3D microparticles,” *Opt. Express* **26**(10), 13543 (2018).
- [9] Webber, D., Zhang, Y., Picard, M., Boisvert, J., Paquet, C. and Orth, A., “Versatile volumetric additive manufacturing with 3D ray tracing,” *Opt. Express* **31**(4), 5531 (2023).
- [10] Boniface, A., Maître, F., Madrid-Wolff, J. and Moser, C., “Volumetric helical additive manufacturing,” *Light: Advanced Manufacturing* **4**(2), 1 (2023).
- [11] Orlov, S., “Theory of three-dimensional reconstruction 1. Conditions for a complete set of projections,” *Soviet Physics Crystallogr.* **20**, 312–314 (1976).
- [12] Toombs, J. and Taylor, H. K., “Design of a tomographic projection lithography process for roll-to-roll fabrication of 3D microstructures,” *Novel Patterning Technologies 2021*(February), E. M. Panning and J. A. Liddle, Eds., 11, SPIE (2021).
- [13] Li, C. C., Toombs, J., Taylor, H. K. and Wallin, T. J., “Tomographic projection optimization for volumetric additive manufacturing with general band constraint Lp-norm minimization,” arXiv (2023).
- [14] Toombs, J. T., Shan, I. K. and Taylor, H. K., “Ethyl Cellulose-Based Thermoreversible Organogel Photoresist for Sedimentation-Free Volumetric Additive Manufacturing,” *Macromol. Rapid Commun.* **44**(7), 2200872 (2023).
- [15] Sreedhar, N., Thomas, N., Al-Ketan, O., Rowshan, R., Hernandez, H., Abu Al-Rub, R. K. and Arafat, H. A., “3D printed feed spacers based on triply periodic minimal surfaces for flux enhancement and biofouling mitigation in RO and UF,” *Desalination* **425**(September), 12–21 (2018).
- [16] Al-Ketan, O. and Abu Al-Rub, R. K., “Multifunctional Mechanical Metamaterials Based on Triply Periodic Minimal Surface Lattices,” *Advanced Engineering Materials* **21**(10), 1–39 (2019).
- [17] Rastegarzadeh, S. and Huang, J., “STL-Free Adaptive Slicing Scheme for Additive Manufacturing of Cellular Materials,” *Journal of Computing and Information Science in Engineering*, 1–26 (2023).
- [18] Wade, C., Williams, G., Connelly, S., Kopec, B. and MacCurdy, R., “OpenVCAD: An open source volumetric multi-material geometry compiler,” *Additive Manufacturing* **79**, 103912 (2024).

[19] Greener, J., Pearson, G. and Cakmak, M., eds., [Roll-to-Roll Manufacturing], John Wiley & Sons, Inc., Hoboken, NJ, USA (2018).